Turbulent Swirling Jet Diffusion Flames

AMNON CHERVINSKY*
Israel Institute of Technology, Haifa, Israel

The phenomenological boundary-layer equations describing the flowfield in a turbulent jet diffusion flame with swirl are solved in the von Mises plane. The expressions found are compared with experimental results for three jet flames with different degrees of swirl using semi-empirical values of turbulent exchange coefficients in the flame. The combined theoretical and experimental study indicates that an increase of the swirling motion in a flame leads to an increase of the flame width and mass entrainment and to a corresponding decrease of the flame length. These effects are associated with changes of the values of the turbulent eddy viscosity and Prandtl number caused by varying the swirl intensity in the flame.

Nomenclature

$b_{1/2}$ = flame width defined in the text, Eq. (33)
c = empirical constant defined by Eq. (20)
G_x = axial flux of linear momentum
G_ϕ = axial flux of angular momentum
$c_{p,i}$ = specific heat at constant pressure of species i
D_s = distance from the burner outlet at which the flame is stabilized
E = empirical constant defined by Eq. (31)
H_1 = empirical constant defined by Eq. (27)
H_2 = empirical constant defined by Eq. (30)
h = specific enthalpy
h_i° = standard heat of formation per unit mass of species i at temperature T°
$\bar{L}$ = L/R = flame length
Le^t = turbulent Lewis number
M_k = function defined by Eq. (11)
P = static pressure
Pr^t = turbulent Prandtl number
q° = heat of reaction
r = radial coordinate
R = radius of burner exit
S = $G_\phi/G_x \cdot R$ = degree of swirl
Sc^t = turbulent Schmidt number
T = temperature
u = axial velocity
V = mass flow rate
v = radial velocity
w = swirl velocity
w_i = molecular weight of species i
x = axial coordinate
Y_i = mass fraction of species i
ϵ_i = rate of production of species i by chemical reactions
$\bar{\mu}^t$ = dimensionless turbulent eddy viscosity
ξ_k = dimensionless axial coordinate
ρ = density
ϕ = ratio of initial concentration of fuel to oxidizer
ψ = dimensionless stream function
$\bar{\Gamma} = \bar{r}\bar{w}$, $\omega = \bar{\Gamma}/\psi$ = vorticity

Subscripts

c = centerline values
co = centerline values at burner exit
e = value in stagnant surroundings
F = fuel
f = flame surface
k = index of generalized variables
i = pertinent to concentration
m = maximum value
mo = maximum value at burner exit
T = pertinent to enthalpy
u = pertinent to velocity
L = flame tip value
ox = oxidizer
I = value in the oxygen free region
II = value in the fuel free region

Received August 28, 1968; revision received February 24, 1969.

* Lecturer, Department of Aeronautical Engineering, Technion I.I.T.; now Research Associate, Department of Aerospace and Mechanical Sciences, Princeton University, Princeton, N.J. Member AIAA.

I. Introduction

THE effect of swirling motion on jet diffusion flames has been investigated previously.[1-4] In those investigations it was shown that swirl leads to a faster decay of the axial velocity, and to an increase of the flame width and mass entrainment in the downstream direction as compared to nonswirling flames. It was also found that flame length decreases when the swirling motion is intensified.

In the aforementioned papers and in other works[5-7] dealing with nonswirling flames, a theoretical approach based essentially on the assumption of similarity of the velocity and temperature profiles in consecutive cross sections was employed. When compared with experimental results, good agreement between the measured and predicted axial velocity distributions was found, whereas only qualitative agreement for the temperature profiles was obtained. It seems that the existence of two regions in the flame separated by some kind of a flame surface, and whose nature is very different (the temperature increases in the inner region while a fast decrease takes place in the outer regions), does not allow for the formation of affine profiles along the flame axis in the important zone where chemical reactions take place.

In the present analysis the boundary-layer equations of motion for a turbulent jet diffusion flame with swirl are solved in the von Mises plane. The nonsimilar solutions obtained give the distribution of axial and swirl velocities and of the temperature and species mass concentration in the flame. The theoretical expressions are compared with measurements of velocity and temperature in flames with different degrees of swirl and fair agreement is found. The comparison is performed under the assumption of a one-step chemical reaction occurring at a flame surface. The analysis shows that the effect of swirl on the flame may be connected with the rise of the value of the turbulent eddy viscosity and the variation of the turbulent Prandtl number in the flame with increasing swirl.

II. Analysis

In a cylindrical coordinate system (r, ϕ, x) the boundary-layer equations describing the stationary flowfield of an axi-

symmetrical turbulent jet diffusion flame with swirl are

$$\frac{\partial}{\partial x}(\rho u r) + \frac{\partial}{\partial r}(\rho v r) = 0 \tag{1a}$$

$$\rho u \frac{\partial u}{\partial x} + \rho v \frac{\partial u}{\partial r} = \frac{1}{r}\frac{\partial}{\partial r}\left(\mu^t r \frac{\partial u}{\partial r}\right) \tag{1b}$$

$$\rho u \frac{\partial \Gamma}{\partial x} + \rho v \frac{\partial \Gamma}{\partial r} = \frac{1}{r}\frac{\partial}{\partial r}\left[\mu^t\left(r\frac{\partial \Gamma}{\partial r} - 2\Gamma\right)\right] \tag{1c}$$

$$\rho u \frac{\partial h}{\partial x} + \rho v \frac{\partial h}{\partial r} = \frac{1}{r}\frac{\partial}{\partial r}\left(\frac{\mu^t}{Pr^t} r \frac{\partial h}{\partial r}\right) - \sum_{i=1}^{N} h_i{}^{\circ}\epsilon_i \tag{1d}$$

$$\rho u \frac{\partial Y_i}{\partial x} + \rho v \frac{\partial Y_i}{\partial r} = \frac{1}{r}\frac{\partial}{\partial r}\left(\frac{\mu^t}{Sc^t} r \frac{\partial Y_i}{\partial r}\right) + \epsilon_i, \quad i = 1,2,\ldots,n \tag{1e}$$

In deriving Eqs. (1) it was assumed that the turbulent Lewis number equals unity, body forces and radiation effects are negligible, and the diffusion of the various species in the flame is governed by Fick's law. The use of turbulent phenomenological transfer coefficients implies further that the turbulence intensity is low. As may be found by an ordering procedure (carried out partly in Ref. 8), the neglect of pressure gradients and the application of the boundary-layer approximations to swirling flows limit the following analysis to cases of weak and moderate degrees of swirl. In these cases the ratio of the swirl velocity to axial velocity, w/u, is assumed to be of the order of δ and $\delta^{1/2}$, respectively, where δ is the ratio of the radial to axial length scales for the nonswirling jet, which is of the order of 0.1.

In addition to Eqs. (1a–1e) we assume a one-step chemical reaction to take place,

$$\sum_{i=1}^{N} \nu'_i M_i \rightarrow \sum_{i=1}^{N} \nu''_i M_i \tag{1f}$$

so that in this case the reaction rate $\epsilon = \epsilon_i/w_i(\nu''_i - \nu'_i)$ is the same for all the species.

Equations (1b, 1d, and 1e) can be cast into a common form

$$\rho u \frac{\partial Q_k}{\partial x} + \rho v \frac{\partial Q_k}{\partial r} = \frac{1}{r}\frac{\partial}{\partial r}\left(\mu^t \cdot A_k r \frac{\partial Q_k}{\partial r}\right) \tag{2}$$

where Q_k is equal to u, to

$$\beta_T = h \Big/ \sum_{i=1}^{N} h_i{}^{0} w_i(\nu'_i - \nu''_i) - \alpha_1$$

or to $\beta_i = Y_i/w_i(\nu''_i - \nu'_i) - \alpha_1$ in Eqs. (1b, 1d, and 1e), respectively, and α_1 is a particular solution of Eq. (1e). A_k equals 1, $1/Pr^t$, or $1/Sc^t = 1/Pr^t$ corresponding to Eqs. (1b, 1d, and 1e), respectively.

Define a dimensionless stream function so that

$$\bar{\rho}\bar{u}\bar{r} = \frac{\partial}{\partial \bar{r}}\left(\frac{\psi^2}{4}\right), \quad \bar{\rho}\bar{v}\bar{r} = -\frac{\partial}{\partial \bar{x}}\left(\frac{\psi^2}{4}\right)$$

where

$$\bar{x} = x/R, \ \bar{r} = r/R, \ \bar{u} = u/u_{co}, \ \bar{v} = v/u_{co}$$

$$\bar{\mu}^t = \mu^t/\rho_{co}u_{co}R, \ \bar{\Gamma} = \Gamma/Ru_{co}, \ \bar{\rho} = \rho/\rho_{co}$$

The equation of continuity is then satisfied identically in terms of the defined stream function.

Performing a transformation from the physical plane $(\bar{x}, \bar{r})$ to the von Mises plane (η,ψ), where

$$\eta = \bar{x}, \ \bar{r}^2 = \int_0^{\psi} \frac{\psi' d\psi'}{\bar{\rho}\bar{u}} \tag{3}$$

Eqs. (2) and (1c) may be written in a dimensionless form in the transformation plane as follows:

$$\frac{\partial Q_k}{\partial \eta} = \frac{4}{\psi}\frac{\partial}{\partial \psi}\left(\frac{A_k \cdot \bar{\mu}^t \cdot \bar{\rho}\bar{u}\bar{r}^2}{\psi}\frac{\partial Q_k}{\partial \psi}\right) \tag{4}$$

$$\frac{\partial \bar{\Gamma}}{\partial \eta} = \frac{4}{\psi}\frac{\partial}{\partial \psi}\left(\frac{\bar{\mu}^t \cdot \bar{\rho}\bar{u}\bar{r}^2}{\psi}\frac{\partial \bar{\Gamma}}{\partial \psi} - \bar{\mu}^t\bar{\Gamma}\right) \tag{5}$$

In the vicinity of the axis $\bar{\rho}\bar{u}\bar{r}^2$ may be expanded in powers of ψ about an axial station $(\eta, 0)$,

$$\bar{\rho}\bar{u}\bar{r}^2(\eta,\psi) = \bar{\rho}\bar{u}\bar{r}^2(\eta,0) + \psi\left[\frac{\partial}{\partial \psi}(\bar{\rho}\bar{u}\bar{r}^2)\right]_{\eta,0} + \frac{\psi^2}{2}\left[\frac{\partial^2}{\partial \psi^2}(\bar{\rho}\bar{u}\bar{r}^2)\right]_{\eta,0} + \ldots$$

Direct computation shows[9] that

$$\bar{\rho}\bar{u}\bar{r}^2(\eta,0) = \left[\frac{\partial}{\partial \psi}(\bar{\rho}\bar{u}\bar{r}^2)\right]_{\eta,0} = \left[\frac{\partial^3}{\partial \psi^3}(\bar{\rho}\bar{u}\bar{r}^2)\right]_{\eta,0} = 0$$

$$[(\partial^2/\partial\psi^2)(\bar{\rho}\bar{u}\bar{r}^2)]_{\eta,0} = 1$$

so that $\bar{\rho}\bar{u}\bar{r}^2(\eta,\psi) \cong \frac{1}{2}\psi^2$ neglecting 4th- and higher-order terms.

Introducing the approximation found, and assuming further that $A_k\mu^t$ are functions of the axial distance only, one obtains finally from Eqs. (4) and (5),

$$\frac{\partial M_k}{\partial \xi_k} = \frac{\partial^2 M_k}{\partial \psi^2} + \frac{1}{\psi}\frac{\partial M_k}{\partial \psi} \tag{4a}$$

$$\frac{\partial \omega}{\partial \xi_k} = \frac{\partial^2 \omega}{\partial \psi^2} + \frac{1}{\psi}\frac{\partial \omega}{\partial \psi} - \frac{\omega}{\psi^2} \tag{5a}$$

where

$$M_k = (Q_k - Q_{ke})/(Q_{kco} - Q_{ke}), \ \bar{\Gamma} = \omega\psi$$

and

$$\xi_k = 2\int_0^{\eta} A_k(\eta')\bar{\mu}^t(\eta')d\eta' \tag{6}$$

Equations (4a) and (5a) are to be solved subject to the following side conditions:

$$M_k(\xi_k,0) < \infty, \ \omega(\xi_k,0) = 0$$

$$\lim_{\psi\to\infty} M_k(\xi_k,\psi) = \lim_{\psi\to\infty} \psi M_k(\xi_k,\psi) = 0$$

$$\lim_{\psi\to\infty} \omega(\xi_k,\psi) = \lim_{\psi\to\infty} \psi\omega(\xi_k,\psi) = 0$$

and the initial conditions,

$$M_k(0,\psi) = \begin{cases} 1 & 0 \leqslant \psi \leqslant \psi_0 \\ 0 & \psi_0 < \psi \end{cases} \qquad \omega(0,\psi) = \begin{cases} \omega_0\psi & 0 \leqslant \psi \leqslant \psi_0 \\ 0 & \psi_0 < \psi \end{cases}$$

where ψ_0 corresponds to the radius of the burner in the von Mises plane and is found from Eq. (3),

$$\bar{r}^2 = 1 = \int_0^{\psi_0} \psi' d\psi' = \frac{\psi_0{}^2}{2}$$

since of course at the outlet $\bar{r}^2 = \bar{\rho} = \bar{u} = 1$. The preceding initial conditions imply a uniform distribution of axial velocity, enthalpy, and species mass concentration, and a tangential velocity resulting from solid body rotation at the outlet.

Equation (4a) together with the side and initial conditions can be solved employing the zeroth-order Hankel transform

$$\tilde{R}(\xi_k,z) = \int_0^{\infty} \psi R(\xi_k,\psi)J_0(z\psi)d\psi \tag{7}$$

having the inverse

$$R(\xi_k,\psi) = \int_0^\infty z\tilde{R}(\xi_k,z)J_0(z\psi)dz \tag{7a}$$

Introducing

$$R(\xi_k,\psi) \equiv \partial^2 M_k/\partial\psi^2 + (1/\psi)\partial M_k/\partial\psi$$

into Eq. (7) and performing the integration, one obtains

$$\tilde{R}(\xi_k,z) = -z^2\tilde{M}_k(\xi_k,z)$$

and since $R(\xi_k,\psi)$ is equal also to $\partial M_k/\partial\xi_k$ [see Eq. (4a)] we find

$$\partial\tilde{M}_k/\partial\xi_k + z^2\tilde{M}_k = 0 \tag{8}$$

A formal solution of Eq. (8) is given by

$$\tilde{M}_k(\xi_k,z) = A(z)\exp(-z^2\xi_k) \tag{9}$$

and the inverse transformation (7a) yields

$$M_k(\xi_k,\psi) = \int_0^\infty zA(z)\exp(-z^2\xi_k)J_0(z\psi)dz \tag{10}$$

The function $A(z)$ is determined with the aid of the initial condition

$$M_k(0,\psi) = \int_0^\infty zA(z)J_0(z\psi)dz$$

and applying the inverse transformation

$$A(z) = \int_0^\infty \psi M_k(0,\psi)J_0(z\psi)d\psi = \int_0^{\psi_0}\psi J_0(z\psi)d\psi$$

so that the general solution becomes

$$M_k(\xi_k,\psi) = \int_0^\infty z\exp(-z^2\xi_k)J_0(z\psi)dz\int_0^{\psi_0}\psi' J_0(z\psi')d\psi'$$

Changing the order of integration and using the Weber integral

$$\int_0^\infty e^{-ct^2}J_n(at)J_n(bt)tdt = \frac{1}{2c}\exp\left(-\frac{a^2+b^2}{4c}\right)I_n\left(\frac{ab}{2c}\right)$$

the form of the general solution is modified to

$$M_k(\xi_k,\psi) = \frac{1}{2\xi_k}\exp\left(-\frac{\psi^2}{4\xi_k}\right)\int_0^{\psi_0}\psi'\exp\left(-\frac{\psi'^2}{4\xi_k}\right)\times I_0\left(\frac{\psi\psi'}{2\xi_k}\right)d\psi' \tag{11}$$

In a similar way using the first-order Hankel transform

$$\tilde{S}(\xi_k,z) = \int_0^\infty \psi S(\xi_k,\psi)J_1(z\psi)d\psi \tag{12}$$

and its inverse, the final solution of Eq. (5a) is found to be

$$\omega(\xi_k,\psi) = \frac{\omega_0}{2\xi_k}\exp\left(-\frac{\psi^2}{4\xi_k}\right)\int_0^{\psi_0}\psi'^2\exp\left(-\frac{\psi'^2}{4\xi_k}\right)I_1\times\left(\frac{\psi\psi'}{2\xi_k}\right)d\psi' \tag{13}$$

Setting

$$\lambda = \psi_0/(2\xi_k)^{1/2},\ \chi = \psi/(2\xi_k)^{1/2}$$

let $P_0(\lambda,0) = 1 - \exp(-\lambda^2/2)$, and define $P^*(\lambda,\chi) = P(\lambda,\chi)/P_0(\lambda,0)$, then Eq. (11) becomes

$$M_k(\xi_k,\psi) = P_0(\lambda,0)\cdot P^*(\lambda,\chi) = \left[1-\exp\left(\frac{-\psi_0^2}{4\xi_k}\right)\right]P^*\left(\frac{\psi_0}{(2\xi_k)^{1/2}};\ \frac{\psi}{(2\xi_k)^{1/2}}\right) \tag{14}$$

Integrating Eq. (13) by parts making use of the recurrence formula $I_1(\tau) + \tau I_1'(\tau) = \tau I_0(\tau)$, one obtains

$$\omega(\xi_k,\psi) = \omega_0\psi\left[1-\exp\left(\frac{-\psi_0^2}{4\xi_k}\right)\right]\times\left[P^*\left(\frac{\psi_0}{(2\xi_k)^{1/2}};\ \frac{\psi}{(2\xi_k)^{1/2}}\right) - Q^*\left(\frac{\psi_0}{(2\xi_k)^{1/2}};\ \frac{\psi}{(2\xi_k)^{1/2}}\right)\right] \tag{15}$$

where

$$Q^*(\lambda,\chi) = \frac{(\lambda/\chi)I_1(\lambda,\chi)\exp[(-\lambda^2+\chi^2)]/2}{1-\exp(-\lambda^2/2)}$$

The functions $P_0(\lambda,0)$ and $P^*(\lambda,\chi)$ have been tabulated by Masters.[10] The function Q^* has been evaluated in Ref. 11 so that $\omega(\xi_k,\psi)$ is easily calculated.

Along the axis ($\psi = 0$) $P^*(\psi_0/(\xi_k)^{1/2},\ \psi/(2\xi_k)^{1/2}) = 1$,

$$M_k(\xi_k,0) = 1 - \exp(-\psi_0^2/4\xi_k) \tag{16}$$

and $\omega(\xi_k,0) = 0$. Equation (11), or its modified form Eq. (14), describes the distribution of the axial velocity $\bar{u}$ in the form of

$$\bar{u} = u/u_{co} = M_u(\xi_u,\psi) \tag{17}$$

and from (16)

$$u_c/u_{co} = 1 - \exp -(1/2\xi_u) \tag{17a}$$

since $Q_{ke} = u_e = 0$ in the stagnant surroundings.

The variation of the swirl velocity in the flame is expressed via the distribution of the vorticity by Eq. (13) or (15) when substituting $\bar{\Gamma} = \bar{r}\bar{w} = \psi\omega(\xi_k,\psi)$.

The general equation (11) gives also the distribution of the enthalpy variable β_T and the mass concentration variable β_i as defined in relation to Eq. (2). Equation (16) yields the distribution of these terms along the flame axis.

In diffusive flames fuel is usually injected as a jet into the surrounding atmosphere, which supplies the oxidizer. We shall take in Eq. (1f) $\nu'_1 = \nu_{\text{fuel}}$, $\nu'_2 = \nu_{\text{ox}}$ and therefore

$$\alpha_1 = \alpha_F = -Y_F/\nu_F w_F,\ \beta_T = h/q_0 + Y_F/\nu_F w_F$$

$$\beta_{\text{ox}} = \alpha_{\text{ox}} - \alpha_F = -Y_{\text{ox}}/\nu_{\text{ox}}w_{\text{ox}} + Y_F/\nu_F w_F$$

Assuming that the chemical reaction is confined to a flame surface, where it occurs instantaneously, this surface must divide the flowfield into two regions. In the inner region, denoted by subscript I, no oxidizer is present and, therefore, $\beta_{\text{ox,I}} = Y_F/\nu_F w_F$. In the other region, identified by subscript II, no fuel is present ($Y_{F,\text{II}} = 0$) so that $\beta_{\text{ox,II}} = -Y_{\text{ox}}/\nu_{\text{ox}}w_{\text{ox}}$. Equation (11) with $Q_k \equiv \beta_i$ thus describes the distribution of fuel concentration in region I (between the axis of symmetry and the flame surface) and the distribution of oxidizer in region II (from the flame surface outwards). Since $\beta_{\text{ox},e} = -(Y_{\text{ox}}/\nu_{\text{ox}}w_{\text{ox}})_e$ and $\beta_{\text{ox},co} = (Y_F/\nu_F w_F)_{co}$, we obtain from Eq. (11) for the concentration of fuel

$$\frac{Y_F}{\nu_F w_F}\Big/\left(\frac{Y_F}{\nu_F w_F}\right)_{co} = -\frac{1}{\phi} + \left(1+\frac{1}{\phi}\right)M_i(\xi_i,\psi) \tag{18}$$

and along the axis

$$\left(\frac{Y_F}{\nu_F w_F}\right)_c\Big/\left(\frac{Y_F}{\nu_F w_F}\right)_{co} = 1 - \left(1+\frac{1}{\phi}\right)\exp\left(-\frac{1}{2\xi_i}\right) \tag{18a}$$

where

$$\phi = \left(\frac{Y_F}{\nu_F w_F}\right)_{co}\Big/\left(\frac{Y_{\text{ox}}}{\nu_{\text{ox}}w_{\text{ox}}}\right)_e$$

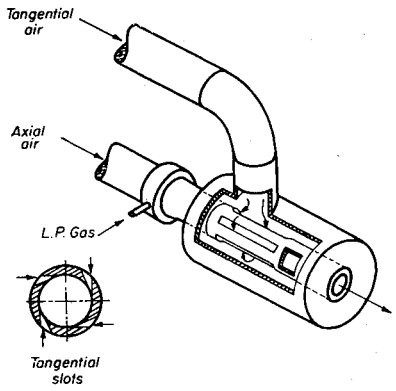

Fig. 1 Swirl burner.

The concentration of oxidizer in the external region is given by

$$\frac{Y_{ox}}{\nu_{ox}w_{ox}}\Big/\left(\frac{Y_{ox}}{\nu_{ox}w_{ox}}\right)_e = 1 - (\phi + 1)M_i(\xi_i,\psi) \qquad (19)$$

Employing the flame surface model, the fuel mass concentration must vanish at the surface. Hence setting $Y_F = 0$ in Eq. (18) provides a relation between ξ_i and ψ_f which defines the locus of the flame surface,

$$\frac{1}{\phi + 1} = \frac{1}{2\xi_i}\exp\left(-\frac{\psi_f^2}{4\xi_i}\right)\int_0^{(2)^{1/2}} \times \exp\left(-\frac{\psi'^2}{4\xi_i}\right) I_0\left(\frac{\psi_f\psi'}{2\xi_i}\right)\psi' d\psi' \qquad (20)$$

The flame length is then given by substituting into Eq. (20) the condition that the flame tip lies on the axis of symmetry ($\psi_f = 0$),

$$\xi_L = \frac{\frac{1}{2}}{\ln(1 + 1/\phi)} = 2\int_0^{\bar{L}} \frac{\bar{\mu}^t(\bar{x})d\bar{x}}{Pr^t(\bar{x})} \qquad (21)$$

The distribution of enthalpy is given by Eq. (11) for $Q_k = \beta_T$. In this case

$$\beta_T = h/q^\circ + Y_F/\nu_F w_F,\ \beta_{Te} = h_e/q^\circ$$

(because $Y_{Fe} = 0$) and

$$\beta_{Tco} = (h/q^\circ + Y_F/\nu_F w_F)_{co}$$

where

$$h = \int_{T^\circ}^{T} c_p\, dT$$

and T° is a reference temperature usually taken as 298.16°K. If $T_e = T^\circ$ and the gaseous fuel emerges from the orifice at the same temperature, Eq. (11) yields

$$\left(\frac{h/q^\circ}{(Y_F/\nu_F w_F)_{co}}\right)_{\mathrm{I}} = -\frac{Y_F/\nu_F w_F}{(Y_F/\nu_F w_F)_{co}} + M_T(\xi_T,\psi) \qquad (22)$$

$$\left(\frac{h/q^\circ}{(Y_F/\nu_F w_F)_{co}}\right)_{\mathrm{II}} = M_T(\xi_T,\psi) \qquad (22a)$$

The enthalpy variation along the axis is given by

$$\left(\frac{h_c/q^\circ}{(Y_F/\nu_F w_F)_{co}}\right)_{\mathrm{I}} = -\frac{(Y_F/\nu_F w_F)_c}{(Y_F/\nu_F w_F)_{co}} + 1 - \exp\left(-\frac{1}{2\xi_T}\right) \qquad (23)$$

$$\left(\frac{h_c/q^\circ}{(Y_F/\nu_F w_F)_{co}}\right)_{\mathrm{II}} = 1 - \exp\left(-\frac{1}{2\xi_T}\right) \qquad (23a)$$

III. Experimental Results and Discussion

Air was introduced axially and tangentially through four tangential slots into the swirl burner (Fig. 1) and the degree of swirl was changed by varying independently the axial and tangential flow rates. Liquefied petroleum gas was evaporated in a heat exchanger and introduced into the system in the gaseous phase. The gas/air mixture was issued from the 50-mm diam burner orifice with a velocity of the order of 100 m/sec and was ignited by means of a pilot flame. For a distance of 250 cm the flame was unconfined and air was entrained from the stagnant surroundings.

Measurements of the flow rates of air and fuel gas were made with the aid of sharp-edged orifice plates. Time mean values of velocity and static pressure and of temperature were determined employing a 5-hole hemispherical water cooled impact probe and a Pt–Pt 13% Rh thermocouple.

The impact probe developed by Lee and Ash[12] was calibrated in a wind tunnel over a range of yaw and pitch angles. Coating of the thermocouple bead against catalytic effects and corrections of temperature readings due to radiation losses were carried out according to methods described in Ref. 13.

In the present study three flames with a fixed initial fuel/air ratio and different degrees of swirl were investigated. The initial fuel/air ratio was well outside the flammability limits and the degrees of swirl, characterized by the dimensionless swirl number $S = G_\phi/G_x \cdot R$, corresponded to weak and moderate swirl as defined in the analysis.

The chemical reaction is taken as a one-step reaction of LPG burning in air,

$$1\tfrac{1}{2}C_2H_6 + 5C_3H_8 + 3\tfrac{1}{2}C_4H_{10} + 53O_2 + 200N_2 \rightarrow 32CO_2 + 42H_2 + 200N_2 - 5100\ \text{kcal} \qquad (24)$$

Other data used in the computations are $T_0 = 300$°K, $\nu_F w_F = 0.468$ kg, $Y_{ox}/\nu_{ox}w_{oxe} = 0.137$ kg^{-1}, $c_p = 0.45$ kcal/kg °C, $q^\circ = 5100$ kcal.

In order to compare the experimental and analytical results it is necessary to transform the solutions given in Eqs. (17, 18, 22, and 23) to the physical plane with the aid of Eqs. (3) and (6). For the transformation in the axial direction a model expressing $\bar{\mu}^t$ must be provided. Such a model was suggested by Ferri[9,14] as a generalization of the expression of the eddy viscosity in jets given previously by Prandtl. This relation was further extended by the author to flames with swirl[11] and was shown to be expressed by the equation

$$\bar{\mu}^t = k_1 \cdot \bar{\rho}_f^{1/2} \qquad (25)$$

where k_1 is a constant depending on the degree of swirl and $\bar{\rho}_f$ is the dimensionless density corresponding to the flame temperature.

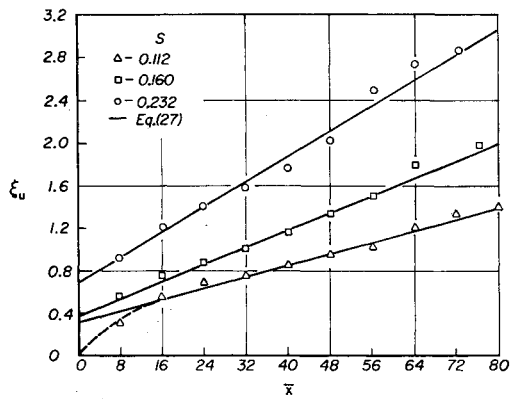

Fig. 2 Transformation in the axial direction, ξ_u vs $\bar{x}$.

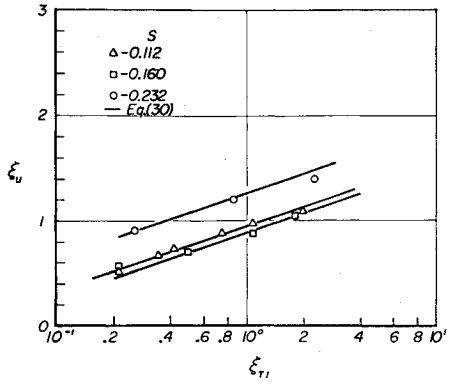

Fig. 3 Transformation in the axial direction, ξ_u vs ξ_T.

Combining Eqs. (6) and (17a) we find $\bar{\mu}^t = \frac{1}{2}d\xi_u/d\bar{x}$ where

$$\xi_u = \frac{1}{2}\left[\ln \frac{1}{1 - u_c(\bar{x})/u_{co}}\right]^{-1} \tag{26}$$

and the index u indicates that this transformation is carried out for the velocity field only where in Eq. (6) $A_k \equiv 1$. Introducing into Eq. (26) the values of the axial velocity measured at various stations on the flame axis and plotting the relations obtained, an expression for ξ_u vs $\bar{x}$ is found. Such a plot for the three flames investigated is shown in Fig. 2, from which one deduces the following empirical relation between ξ_u and $\bar{x}$:

$$\xi_u = 2\bar{\mu}^t.\bar{x} + H_1 \tag{27}$$

where $\bar{\mu}^t$ and H_1 are constants depending on the degree of swirl and are given in Table 1. From the results it is clear that as the degree of swirl is increased a corresponding rise of the constant value of the eddy viscosity is found.

In an analogous way one obtains a relation for the transformation of the temperature field to the physical plane in the axial direction. The relation obtained for $(\xi_T)_I$ vs $\bar{x}$ is given by

$$(\xi_T)_I = \frac{1}{2}\left[\ln \frac{1}{N\theta_c(\bar{x})}\right]^{-1} \tag{28}$$

where

$$\theta_c(\bar{x}) = \frac{T_c - T_o}{T_0}, \quad N = \frac{\bar{c}\, T_0/q^\circ}{(Y_F/\nu_F w_F)_{co}}\cdot\phi$$

and the values of Y_F and ϕ corresponding to the flames investigated are given in Table 1. Introducing these data and the measured values of the temperature on the flame axis into Eq. (28), $(\xi_T)_I$ is calculated as a function of $\bar{x}$. Having obtained the relations between ξ_k and $\bar{x}$ the transformation of the analytical expressions in the axial direction is thus completed. When performing the above calculations it is interesting to note that combining Eqs. (6, 27, and 28) the variation of the turbulent Prandtl number along the flame axis may be expressed in the form of

$$(1/Pr^t)_I = \tfrac{1}{2}\, d(\xi_T)_I/d\xi_u \tag{29}$$

Plotting therefore the values of $(\xi_T)_I$ and ξ_u for the same $\bar{x}$, as found from Eqs. (26) and (28), respectively, in Fig. 3 the following empirical relation is obtained:

$$(\xi_T)_I = \exp[c(\xi_u - H_2)] \tag{30}$$

Table 1 Swirling flame characteristics

$S = G_\phi/G_x \cdot R$	0.112	0.160	0.232
u_{co}, m/sec	76.0	81.5	103.0
w_{mo}, m/sec	16.7	27.0	54.0
Y_{Fo}	0.245	0.245	0.245
ϕ	3.83	3.83	3.83
$\bar{\mu}^t$	0.683×10^{-2}	1.015×10^{-2}	1.5×10^{-2}
H_1	0.31	0.37	0.68
H_2	0.94	0.88	1.44
c	3.47	3.47	3.47
$\bar{D}_s = D_s/R$	11	6.2	4.0
$\bar{L}_{cal} = (L/R)_{cal}$	61	38	33
$\bar{L}_{exp} = (L/R)_{exp}$	69	51.8	34
T_m°C	1670	1840	1860

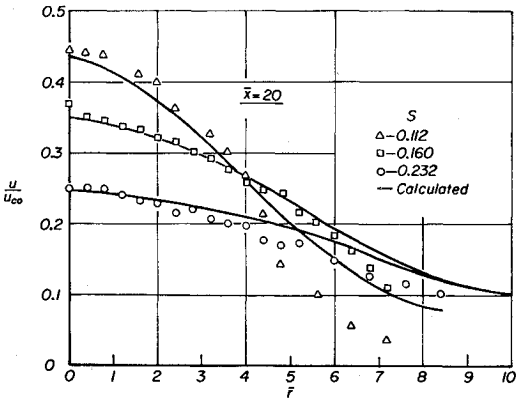

Fig. 4 Radial distribution of axial velocity at $\bar{x} = 20$.

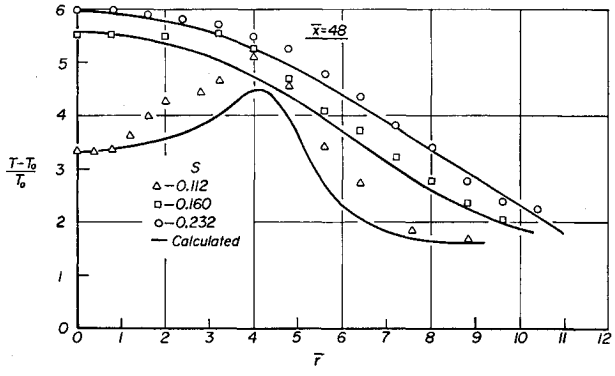

Fig. 5 Radial distribution of temperature at $\bar{x} = 48$.

where c and H_2 are constants given in Table 1 for the various degrees of swirl.

From Eqs. (29) and (30) one derives the following expression for the variation of the turbulent Prandtl number in the inner region of the flame:

$$(1/Pr^t)_I = c\, \exp[c(2\bar{\mu}^t\cdot\bar{x} - E)] \tag{31}$$

where $E = H_1 - H_2$.

The transformation in the radial direction is given by Eq. (3). Using the assumption of constant pressure and $Le^t = 1$, one has $\bar{\rho} = 1/T$ and $\xi_i \equiv \xi_T$. Introducing now the expres-

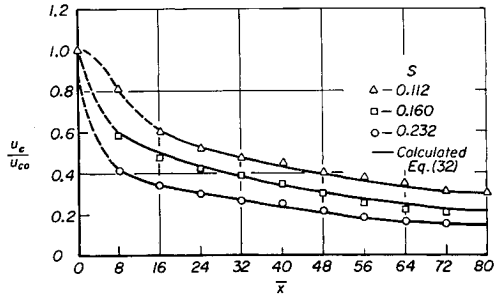

Fig. 6 Decay of axial velocity maximum along the axis.

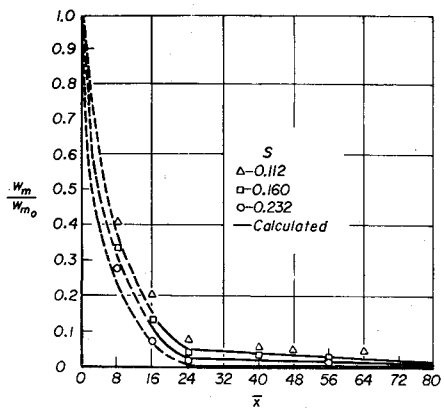

Fig. 7 Decay of swirl velocity maximum along the axis.

sions found in the analysis for $\bar{u}$ and T into Eq. (3), explicit relations connecting the radial coordinates r and ψ can be found for any distance $\bar{x}$ (via ξ_u and ξ_T) in the two regions of the flame.

The retransformed analytical and the measured radial distributions of axial velocity and temperature at $\bar{x} = 20$ and 48 are shown in Figs. 4 and 5, respectively. Fair agreement is seen to exist between the empirical and calculated values. The swirling motion causes a decrease of axial velocity values at the central part of the flowfield leading thus to

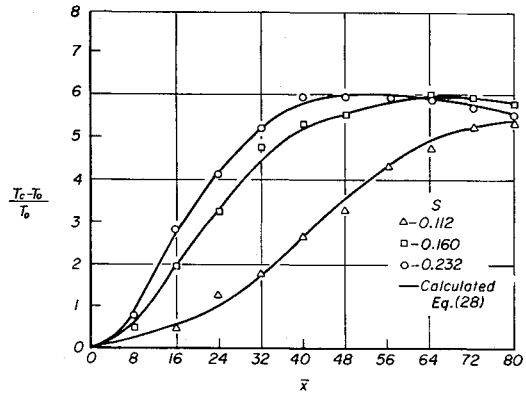

Fig. 8 Variation of temperature on flame axis.

wider velocity profiles as the swirl increases. The same behavior can be observed when the decay of the axial velocity maximum along the axis is plotted in Fig. 6. The equation describing this decay is written after combining Eqs. (17a) and (27) in the form of

$$\frac{u_c}{u_{co}} = 1 - \exp\left[-\frac{1}{2(2\bar{\mu}^t.\bar{x} + H_1)}\right] \tag{32}$$

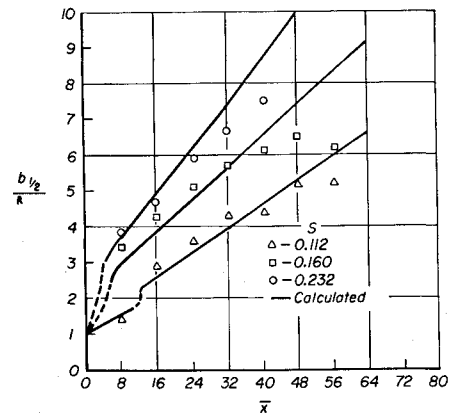

Fig. 9 Variation of flame width along the axis.

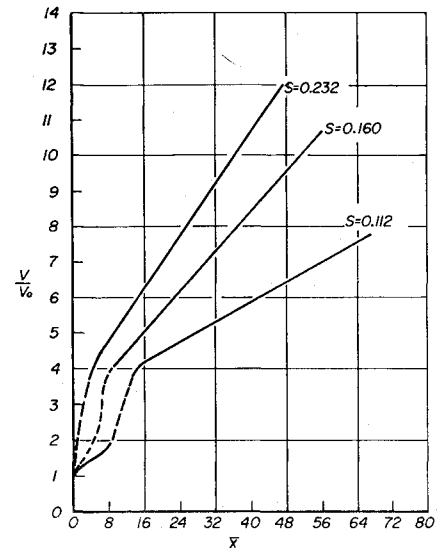

Fig. 10 Mass entrainment along the axis.

As shown in Ref. 8 the cause for the faster decay of axial velocity in the downstream direction when the degree of swirl is increased lies in the shortening of the so-called "potential region" of the jet flow, enabling thus the decay of the velocity to start closer to the burner outlet.

The variation of the swirl velocity maximum and temperature on the flame axis are shown in Figs. 7 and 8, respectively. The temperature increases gradually in the inner region of the flame until it reaches a maximum at the flame tip whose distance from the burner outlet depends on the degree of swirl. The excellent agreement between measured and calculated values in Figs. 6–8 should not be misleading since the experimental constants $\bar{\mu}^t$, H_1, and H_2 were matched so as to fit the experimental data.

The width of the flames investigated in the present work (defined as the distance from the axis of symmetry at which the axial velocity becomes half of its maximum value at the same cross section) is shown in Fig. 9. It seems to vary linearly with the distance from the orifice for all degrees of swirl. The variation of the dimensionless mass entrainment along the axis has been calculated from

$$\frac{V}{V_0} = 2\int_0^{0.5} \bar{\rho}\bar{u}\bar{r}\, d\bar{r} = \frac{\psi^2}{2}\bigg|_{\bar{r}=0.5} \tag{33}$$

and is plotted in Fig. 10.

As can be seen in Fig. 11, the static pressure on the flame axis decays very fast, so that already at a distance of 12 orifice radii it becomes practically equal to the atmospheric pressure. This may be considered a justification of our assumption, made in the analysis, regarding pressure variations in the flame.

Most of the effects of the swirl on the temperature field of the flame is clarified when the flame front lines (which are de-

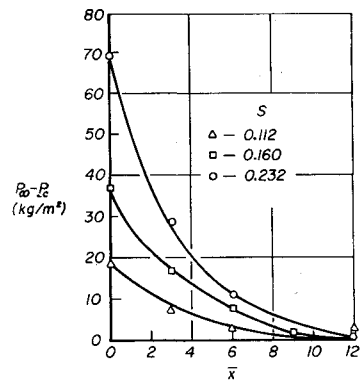

Fig. 11 Decay of static pressure on flame axis.

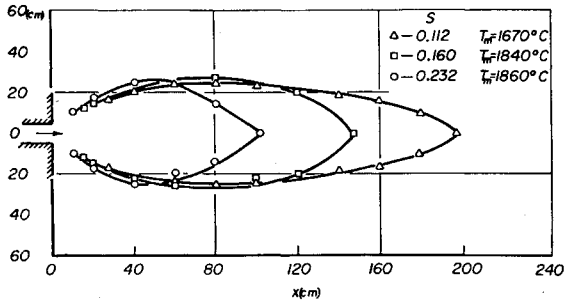

Fig. 12 Flame front lines.

fined here as the locus of the temperature maximum) are plotted (Fig. 12). From the figure it is clear that the length of the flame and the distance from the orifice at which the flame stabilizes decrease markedly with an increase of the degree of swirl. Introducing Eq. (31) into (21) and remembering that $\bar{\mu}^t$ is constant in the flame, the following equation for the flame length is obtained:

$$\bar{L} = \frac{L}{R} = \frac{E + (1/c)\ln[\frac{1}{2}/\ln(1 + 1/\phi)]}{2\bar{\mu}^t} \tag{34}$$

Using the empirical constant values given in Table 1, the flame length is calculated for the various degrees of swirl and compared with the experimental values, as determined from Fig. 12, in Table 1.

Conclusions

The boundary-layer equations describing the conservation of momentum, energy, and species mass concentration in turbulent flames with swirl have been solved in the von Mises plane. After retransforming the solution to the physical plane, it is compared with experimental radial and axial distributions of velocities and temperature in the flame and a fair agreement is obtained.

The introduction of swirl into open jet diffusion flames leads to a faster decay of the velocity, and to an increase of flame width and mass entrainment in the downstream direction as compared to nonswirling flames. In addition, the length of the flame and the distance from the orifice at which the flame is stabilized are shortened significantly when increasing the amount of swirl. All these changes are believed to occur due to two basic causes, which are the reduction of velocity gradients at the burner outlet and the rise of the turbulence intensity level when the degree of swirl S is increased. The first phenomenon leads to the shortening of the potential region near the orifice whereas the other, which is manifested by the increase of the value of the eddy viscosity in the flame, causes a decrease of flame length and surface area. The latter result must be further confirmed by experimental techniques.

References

[1] Beér, J. M. and Chigier, N. A., "Swirling Jet Flames Issuing from an Annular Burner," 5me Journée d'Etudes sur les Flammes, Paris, 1963.

[2] Kerr, N. M. and Fraser, D., "Swirl Part II. Effect on Flame Performance and Modelling of Swirling Flames," *Journal of the Institute of Fuel*, Vol. 38, No. 299, 1965, pp. 519–538.

[3] Chigier, N. A. and Chervinsky, A., "Aerodynamic Study of Turbulent Burning Free Jets with Swirl," *Eleventh International Symposium on Combustion*, The Combustion Institute, Pittsburgh, Pa., 1967, pp. 489–499.

[4] Chervinsky, A. and Timnat, Y. M., "Effect of Swirl on Flame Stabilization," *Israel Journal of Technology*, Vol. 6, 1968, pp. 25–31.

[5] Fay, J. A., "The Distribution of Concentration and Temperature in a Laminar Jet Diffusion Flame," *Journal of the Aeronautical Sciences*, Vol. 21, 1954, pp. 681–689.

[6] Goldburg, A. and Cheng-Sin I., "A Review of the Fluid Dynamic Problem Posed by the Laminar Jet Diffusion Flame," *Combustion and Flame*, Vol. 9, 1965, pp. 259–272.

[7] Kremer, H., "Strömung und Mischung in Frei Brennenden Diffusions Flammen," Ber. 95, 1966, Verein Deutscher Ingenieure, pp. 55–69.

[8] Chigier, N. A. and Chervinsky, A., "Experimental and Theoretical Study of Turbulent Swirling Jets Issuing from a Round Orifice," *Israel Journal of Technology*, Vol. 4, 1966, pp. 44–54.

[9] Kleinstein, G., "An Approximate Solution for the Axisymmetric Jet of a Laminar Compressible Fluid," *Quarterly of Applied Mathematics*, Vol. 20, 1962, pp. 49–64.

[10] Masters, J. I., "Some Applications in Physics of the P-Function," *Journal of Chemical Physics*, Vol. 23, 1955, pp. 1865–1874.

[11] Chervinsky, A., "Aerodynamic Study of Turbulent Jet Flames with Swirl," D.SC. thesis, Technion, Israel Institute of Technology, 1968.

[12] Lee, J. C. and Ash, J. E., "A Three Dimensional Spherical Pitot Probe," *Transactions of the ASME*, Vol. 78, 1956, pp. 603–608.

[13] Kaskan, W. E., "The Dependence of Flame Temperature on Mass Burning Velocity," *Sixth International Symposium on Combustion*, Reinhold, New York, 1957, pp. 134–153.

[14] Ferri, A., Libby, P. A., and Zakkay, V., "Theoretical and Experimental Investigation of Supersonic Combustion," ARL 62-467, Sept. 1962, Polytechnic Institute of Brooklyn.